Proceedings of the ASME 2016 Conference on Smart Materials, Adaptive Structures and Intelligent Systems
SMASIS2016
September 28-30, 2016, Stowe, VT, USA

SMASIS2016-9252

CHARACTERIZATION OF ADAPTIVE MAGNETOELASTIC METAMATERIALS UNDER APPLIED MAGNETIC FIELDS

Ryan L. Harne*, Zhangxian Deng, and Marcelo J. Dapino

Department of Mechanical and Aerospace Engineering
The Ohio State University
Columbus, OH 43210, USA

***Corresponding Author, Email: harne.3@osu.edu**

ABSTRACT

Whether serving as mounts, isolators, or dampers, elastomer-based supports are common solutions to inhibit the transmission of waves and vibrations through engineered systems and therefore help to alleviate concerns of radiated noise from structural surfaces. The static and dynamic properties of elastomers govern the operational conditions over which the elastomers and host structures provide effective performance. Passive-adaptive tuning of properties can therefore broaden the useful working range of the material, making the system more robust to varying excitations and loads. While elastomer-based metamaterials are shown to adapt properties by many orders of magnitude according to the collapse of internal void architectures, researchers have not elucidated means to control these instability mechanisms such that they may be leveraged for on-demand tuning of static and dynamic properties. In addition, while magnetorheological elastomers (MREs) exhibit valuable performance-tuning control due to their intrinsic magnetic-elastic coupling, particularly with anisotropic magnetic particle alignment, the extent of their properties adaptation is not substantial when compared to metamaterials. Past studies have not identified means to apply anisotropic MREs in engineered metamaterials to activate the collapse mechanisms for tuning purposes. To address this limited understanding and effect significant performance adaptation in elastomer supports for structural vibration and noise control applications, this research explores a new concept for magnetoelastic metamaterials (MM) that leverage strategic magnetic particle alignment for unprecedented tunability of performance and functionality using non-contact actuation. MM specimens are fabricated using interrelated internal void topologies, with and without anisotropic MRE materials. Experimental characterization of stiffness, hysteretic loss, and dynamic force transmissibility assess the impact of the design variables upon performance metrics. For example, it is discovered that the mechanical properties may undergo significant adaptation, including two orders of magnitude change in mechanical power transmitted through an MM, according to the introduction of a 3 T free space external magnetic field. In addition, the variable collapse of the internal architectures is seen to tune static stiffness from finite to nearly vanishing values, while the dynamic stiffness shows as much as 50% change due to the collapsing architecture topology. Thus, strategically harnessing the internal architecture alongside magnetoelastic coupling is found to introduce a versatile means to tune the properties of the MM to achieve desired system performance across a broad range of working conditions. These results verify the research hypothesis and indicate that, when effectively leveraged, magnetoelastic metamaterials introduce remarkably versatile performance for engineering applications of vibration and noise control.

1 INTRODUCTION

Structural vibrations and noise deteriorate human health and functionality [1], compromise or destroy system integrity in numerous mechanical, aerospace, civil, and marine applications [2] [3] [4], and prevent the adoption of advanced technologies, for instance due to the creation of environments adverse to sensitive electronics [5]. Because vibrations and sound radiated from mechanical and structural systems are typically unavoidable, the key technologies to address the long-standing concerns are elastomer-based supports (mounts, isolators, dampers, etc.) that inhibit the transmission of waves and vibrations through an engineered system and ultimately alleviate the significance of radiated noise. Such elastomer devices use reactive and resistive phenomena to prevent vibrations from passing through them unabated. The static and dynamic properties of elastomers govern the operational conditions over which the devices provide effective isolation and/or damping performance. Consequently, there is a need to develop and characterize a diverse assortment of elastomer support solutions throughout engineering applications [6] [7].

Balancing the simplicity of passive support materials with the more robust performance of fully-active solutions [8] [9] [10], *passive-adaptive* or semi-active supports facilitate static and dynamic properties tuning through low-complexity and/or self-sufficient actively-switched strategies. Magneto-rheological elastomers (MREs) have emerged as passive-adaptive material systems able to be usefully put to practice in certain applications. MREs are fabricated by mixing iron particles in an elastomer prior to curing. *Isotropic* MREs are made by curing the material in the absence of a magnetic field such that the particles have no particular alignment, while *anisotropic* MREs are fabricated by curing in a magnetic field such that the post-cure MRE is magnetically polarized (creating particle chains). Anisotropic MREs respond preferentially to applied fields. In fact, the anisotropy is shown to be essential to usefully act on the materials for properties adaptation because there is substantially greater influence upon the MRE at the microstructural scale from externally applied magnetic fields [11]. These 'smart materials' have attracted significant attention, particularly in serving as vibration and noise control supports with magnetic field-controlled stiffness modulation [12]. MREs may also be implemented across a wide range of applications [11], and introduce the potential for self-powering the required electronic components using energy that is captured and recycled within the platform [13] [14]. Yet, despite the advantages, the extent of properties tuning is directly related to the applied field, and thus the tuning cannot exceed that provided by the level of applied magnetic which can draw substantial power (much more than can be recycled [11]) if large tuning is demanded. A new method of MRE development is required to take such elastomer support technologies to the next level of performance adaptation.

Using pure elastomer materials, recent advances in cellular, elastic *metamaterials* have shown that orders-of-magnitude worth of static and dynamic properties change may be achieved by leveraging instabilities inherent to strategic internal topology [15] [16]. One such topological transition is compared to traditional, bulk material behavior in Figure 1. In Fig. 1(a) and (b), a conventional MRE specimen deforms under compressive load, exhibiting a positive Poisson's ratio. In contrast, the metamaterial in Fig. 1(c) and (d) contracts laterally under the same compression due to instability associated with collapse of the circular voids. Over the course of this transition, the static mechanical properties of the metamaterial change by many orders of magnitude, including near-zero stiffness close to the instability [16]. Researchers are seeking ways to leverage additional physical phenomena to tailor the performance of these metamaterials. For instance, Tipton et al. [17] embedded permanent magnets into a cellular, elastic metamaterial and applied an external field to force the system into the collapsed state; it was hypothesized that this experimentally observed capability was scalable and useful as an actuation mechanism for topological change. Bayat and Gordaninejad [18] [19] have recently used multiphysics finite element simulations to study the role of isotropic MRE on these collapsing mechanisms for elastic wave transmission control. In the models, the researchers consider cellular metamaterial composed of isotropic MRE; when acted upon by external magnetic fields, the metamaterials may deform or collapse, and thus adjust the bandgap behavior for elastic waves. The computational results suggested that wave transmission amplitude and direction could be modified by the non-contact magnetic field [18] [19]

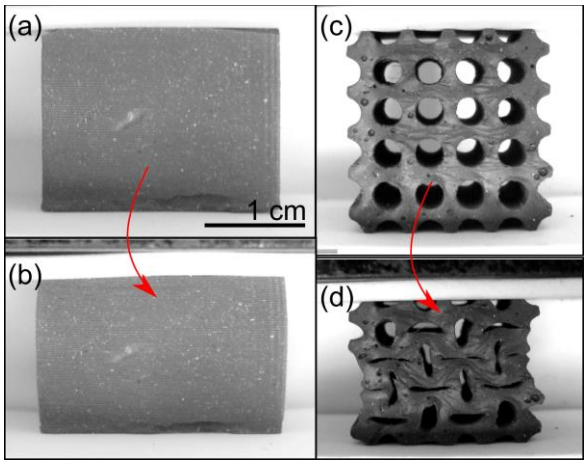

Figure 1. (a,b) CONVENTIONAL MRE AND (c,d) MM IN THE (a,c) UNDEFORMED AND (b,d) COMPRESSED CONFIGURATIONS .

To summarize the developments in the state-of-the-art, passive-adaptive elastomeric support systems have usefully leveraged MRE materials for practical properties (and performance) change, although the greatest adaptation possible in these architectures is limited by the energy available to apply external magnetic fields. Also, despite the discoveries regarding cellular elastic metamaterials and recent computational explorations that incorporate MRE, there is no understanding on how *anisotropic* MRE may govern the properties adaptation of elastic metamaterials and no reported experimental efforts to date that provide a pathway to deliver on the promising opportunities that may be realized via the integration of magnetoelasticity and metamaterials.

2 RESEARCH OBJECTIVE AND OUTLINE

Motivated by the need for passive-adaptive, elastomer supports to tackle vibration and noise concerns in numerous engineering applications, the objective of this research is to advance the state-of-the-art by developing and characterizing *magnetoelastic metamaterials* (MMs) that provide large tunability of performance and functionality using precise, non-contact actuation by magnetic field. By examining both isotropic and anisotropic MRE in the composition of the cellular metamaterials, the aim of this study is to uncover how anisotropic material composition of MMs governs the properties change due to the topological changes. Considering Fig. 1(c) and (d), it is emphasized that the metamaterial is geometrically similar to a grid of elastic squares (or diamonds) connected, via elastic arms, that relatively rotate in response to the compressive stress or applied strain [16]. As a result of this perspective, it is necessary to understand how the relatively-rotating anisotropic

polarizations of the squares will respond to magnetic fields, and how these influences tailor the macroscopically observed properties change of relevance for elastomeric support applications.

The following section details fabrication methods for isotropic and anisotropic MMs. Then, experiments conducted in a load-frame are presented which characterize the mechanical adaptation enabled when the MMs are subjected to external magnetic fields. Finally, investigations are undertaken that uncover how the dynamic properties change due to external magnetic fields and different pre-strains. A summary of findings and future research directions are presented in the last section.

3 MAGNETOELASTIC METAMATERIAL DESIGN AND FABRICATION

To identify the impact of the cellular topology on the MMs, "control" specimens are fabricated using solid MRE for their composition. The fabricated control and MM specimens are shown in Figure 2, in the left and right columns, respectively. Isotropic and anisotropic specimens are created, where the top and bottom rows of Fig. 2 show the isotropic and anisotropic specimens, respectively. By their largest dimensions, each specimen is approximately a cube with side length 20.5 mm; the greatest deviation from these dimensions is about 1 mm.

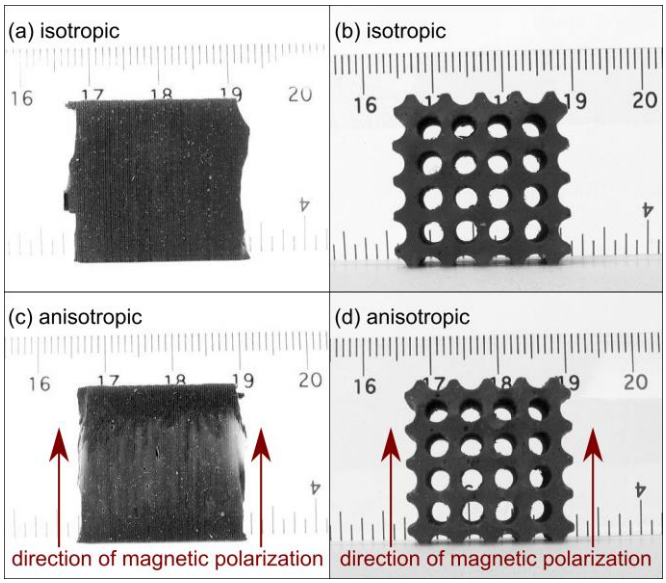

Figure 2. PHOTOGRAPHS OF CONTROL AND MM SPECIMENS. ISOTROPIC SPECIMENS ARE SHOWN IN (a,b), RESPECTIVELY, WHILE THE CORRESPONDING ANISOTROPIC SPECIMENS ARE SHOWN IN (c,d).

The elastomer material used in the creation of the control and MM specimens is Mold Star 15 S (Smooth-On, Inc.) which is a two-part silicone rubber that cures at room temperature via a 1:1 mixture. Once the silicone rubber is sufficiently mixed, carbonyl iron particles (BASF, S-1641) are mixed into the elastomer. The iron particles constitute about 20% of the total volume of the net mixture. Once the iron particles are sufficiently mixed, the resulting uncured MRE is poured into molds. Molds are produced by 3D printing with ABS plastic. For the MM specimens, the molds constitute a base with standing pillars and an outer housing, such that when removed from the mold the MM specimens contains cylindrical voids, such as those shown in Fig. 2(b) and (d).

Once poured into the molds, the isotropic control and MM specimens are allowed to cure for 72 hours before removal from the molds. For the anisotropic specimens, a cap is placed on both molds and sealed with wax; thus the MRE material is fully enclosed within ABS cube molds. Then, on both side of the cubes are placed magnets (Applied Magnets, NB037) of slightly greater cross-section than the specimens inside the cube molds. The magnets are poled through the thickness and are oriented such that a uniform magnetic field of strength approximately 1.32 T is generated within the cubic mold that separates them. These specimens are then allowed to cure for approximately 72 hours before removal from the molds. The anisotropic MM specimen, Fig. 2(d), is magnetized in such a way to align with the direction in which the specimen may collapse when under compressive stress or displacement constraint, Fig. 1(d)

4 MECHANICAL PROPERTIES CHARACTERIZATION

Figure 3 presents the experimental configuration used to characterize the reaction static load and stiffness characteristics of the control MRE and MM specimens under different applied strains. A Test Resources load frame connected with an MLP-50 load cell generates one-dimensional displacements and measures a quasi-static axial force up to 220.5 N along the output shaft direction, shown in Fig. 3 by the double arrow. An MTS grip attaches to the end of the shaft to hold a medium-density fiberboard (MDF) plunger, which delivers a prescribed displacement to the specimens; the use of MDF does not interfere with the force measurements via ferromagnetic influences related to the applied magnetic field. When experiments are conducted with an applied magnetic field, an MDF housing is inserted around the plunger on which the specimen rests and through which the load frame plunger displaces, so that the specimen is at the center of the housing and thus at a location of uniform magnetic field. The housing contains a stack of annular magnets (K&J Magnetics Inc., RZ0X84) that provides a magnetic field of 3.3 T (in free space). The front surface of the plunger attached to the load frame shaft is sprayed with non-reflective paint and then printed with scattered black dots. A digital image correlation (DIC) system tracks the movement of the dots and thus accurately determines the displacement of the plunger, which is considered to be the deformation applied to the specimens. The load frame is operated in a displacement control mode. The strain rates used in this study are 1.3%/s and 1.0%/s for the control and MM specimens, respectively. The maximum compressive loads during each characterization test are selected such that the MM

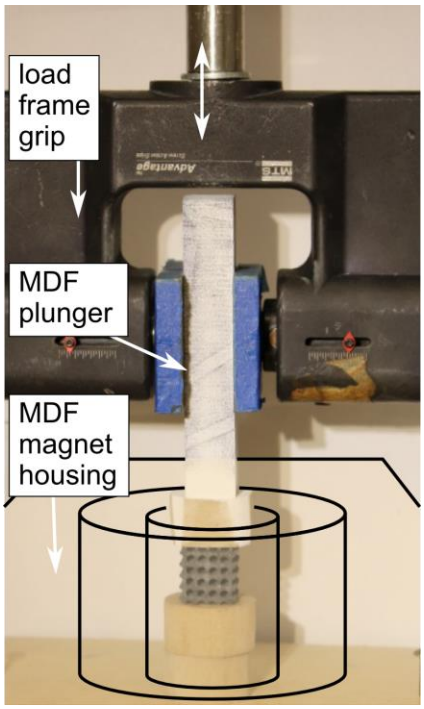

Figure 3. LOAD FRAME EXPERIMENTAL SETUP WITH LOCATION AND MOUNTING OF MAGNETS FOR APPLIED FIELD ILLUSTRATED.

specimen undergoes both local collapse and uniform buckling. All data reported from these quasi-static measurements are taken from the measurements acquired after three full loading and unloading cycles have been conducted. Due to the use of ferromagnetic components near to the applied magnetic field, the influence of the field on the load cell force measurements is identified by conducting tests without specimens in place. Thereafter, and in all data reported herein, this magnetic field influence on the force readings is eliminated to strictly determine the load and stiffness properties of the specimens themselves under the action of the applied displacements. For clarity, all measurements reported below only consider compressive loads and strains upon the specimens, thus strain values indicate the extent compressed from an undeformed configuration.

Figure 4 shows the orientations in which the quasi-static experiments are conducted with respect to the direction of the applied displacement, the direction of the applied magnetic field, and the orientation of the magnetic polarization of the anisotropic specimens. Figure 5(a) compares the force versus displacement profiles for the control MRE specimen with and without magnetic fields. The magnetic field uniformly stiffens the control specimen, whether it is isotropic, Fig. 5(a), or anisotropic, Fig. 5(b). For the control, the stiffness variation is most significant for the isotropic specimen than for the anisotropic specimen that has its polarization in the same axis as the applied magnetic field. The increase in stiffness for the isotropic control specimen is approximately 33% across the entire measurement range of the applied displacement.

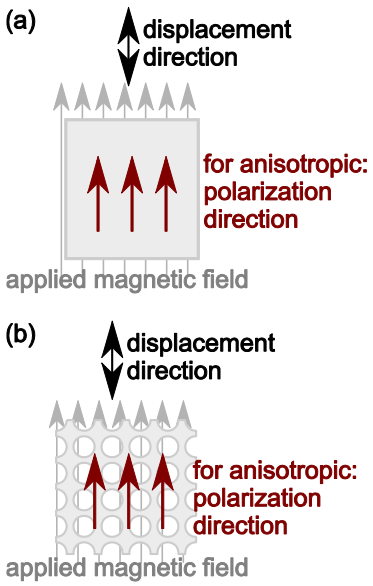

Figure 4. ORIENTATION OF SPECIMENS ACCORDING TO LOAD FRAME DISPLACEMENT DIRECTION, APPLIED MAGNETIC FIELD, AND POLARIZATION OF CORRESPONDING ANISOTROPIC MRE MATERIALS IN THE SPECIMENS.

Figure 5(c) presents the force versus displacement profiles for the isotropic MM specimen with and without magnetic fields. The MM exhibits a linear elastic response for strains less than approximately 10%, with some increasing stiffness appearing in Fig. 5(d) for strains approaching the upper end of this limit. As the strain increases beyond this range, the local collapsing behavior shown in Fig. 1(d) occurs which results in a dramatic reduction in the stiffness, for instance around strain of 19% in Fig. 5(d). The instantaneous stiffness can become so low as to exhibit negative values. For strains beyond this phenomena, the system begins to compact due to self-contact effects and thus the load and instantaneous stiffness both increase substantially. The introduction to the applied magnetic field for the isotropic MM specimen is seen to increase the stiffness of the specimen primarily within the range of applied strains that results in the collapse effect. For the anisotropic specimen, the measurements in Fig. 5(e) and (f) show the external magnetic field has far more dramatic influence on the mechanical properties of the MM. Without a magnetic field, the specimen deforms in a manner very similar to the isotropic specimen, Fig. 5(c). But once the external magnetic field is applied, Fig. 5(e) shows that the specimen immediately collapses and exhibits a nonlinear "hardening" property associated with self-contact, which is why the stiffness shown in Fig. 5(f) for the anisotropic MM specimen under the magnetic field is uniformly increasing. Thus, as shown in Fig. 5(f), turning on and off the external magnetic field can vary the instantaneous stiffness from near-zero values to large finite values on the order of 10 kN/m: a dramatic (and theoretically infinite) extent of stiffness adaptation brought on by the combination of the metamaterial collapsing behavior and the strategic incorporation of the MRE materials.

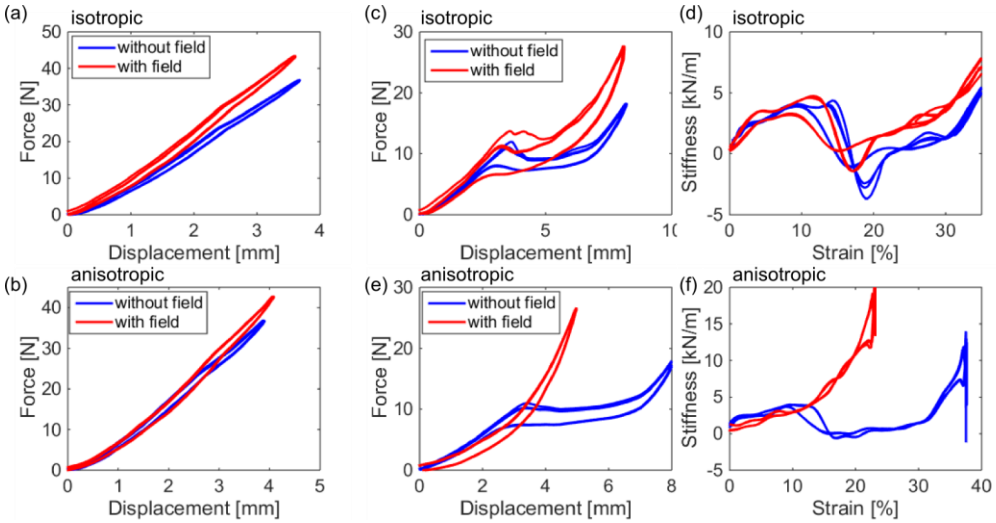

Figure 5. (a,b,c,e) MEASUREMENTS OF REACTION FORCE DUE TO APPLIED DISPLACEMENT. (a,b) RESULTS FOR THE ISOTROPIC AND ANISOTROPIC CONTROL SPECIMENS, RESPECTIVELY; (c,e) RESULTS FOR ISOTROPIC AND ANISOTROPIC MM SPECIMENS, RESPECTIVELY; (d,f) THE DERIVED STIFFNESSES CORRESPONDING TO THE MEASUREMENTS OF THE MM SPECIMENS IN (c,e).

5 DYNAMIC FORCE TRANSMISSIBILITY EVALUATION

Given the significant mechanical adaptation of the MM specimens uncovered in Sec. 4 due to the utilization of the collapsing mechanism and externally-applied magnetic field, force transmissibility experiments were undertaken to study the corresponding dynamic properties change that may be realized via leveraging these two phenomena. In the context of using elastomeric devices for support applications of vibration and noise control, typically the peak force transmitted near a resonance (or mode) is sought to be minimized and one often aims to have this frequency be as low as possible to take advantage of the large transmissibility reduction that occurs force higher frequencies.

The experimental setup is shown in Figure 6(a). An electrodynamic shaker (LDS V408) is fed a slowly-sweeping continuous frequency drive signal which then connects to a force transducer (PCB 208C01) and excitation plunger, Fig. 6(b). The excitation plunger and force transducer are mated with another plunger and force transducer attached to the fixed end of the experimental setup, Fig. 6(b). The plungers are fabricated from MDF so as to have no coupling between them and the applied magnetic field. Prior to the start of a test, the specimens are placed in between the two plungers and given a pre-strain to hold them in place. When experiments are conducted with an applied magnetic field, the same MDF housing and interior annular magnets are employed as those for the mechanical properties characterizations. To account for the impact of the magnets on the experimental hardware, tests are first conducted with no specimen in place, with and without the magnet field. The force transmissibility measurements from these examinations are appropriately subtracted from the measurements taken with specimens in place.

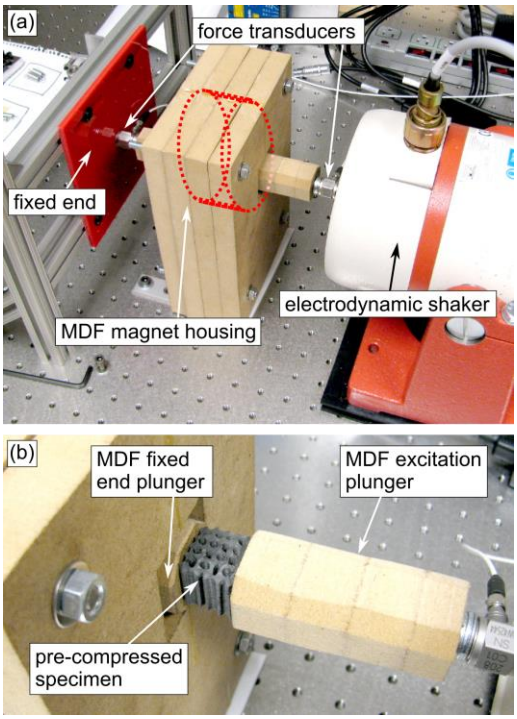

Figure 6. EXPERIMENTAL SETUP FOR CHARACTERIZING DYNAMIC FORCE TRANSMISSIBILITY THROUGH SPECIMENS. (a) PHOTOGRAPH OF FULL SETUP AND (b) ZOOM ON MOUNTING AND STAND-OFF CONDITION FOR THE SPECIMENS COMPRESSED BETWEEN MDF PLUNGERS.

The magnitudes of the force transmissibility measurements for the control specimens are plotted in Figure 7. When an external magnetic field is applied, it is in the axis of polarization of the control specimen, Fig. 7(a). The solid (dotted) curves in Fig. 7(b) and (c) indicate the specimens' responses without (with)

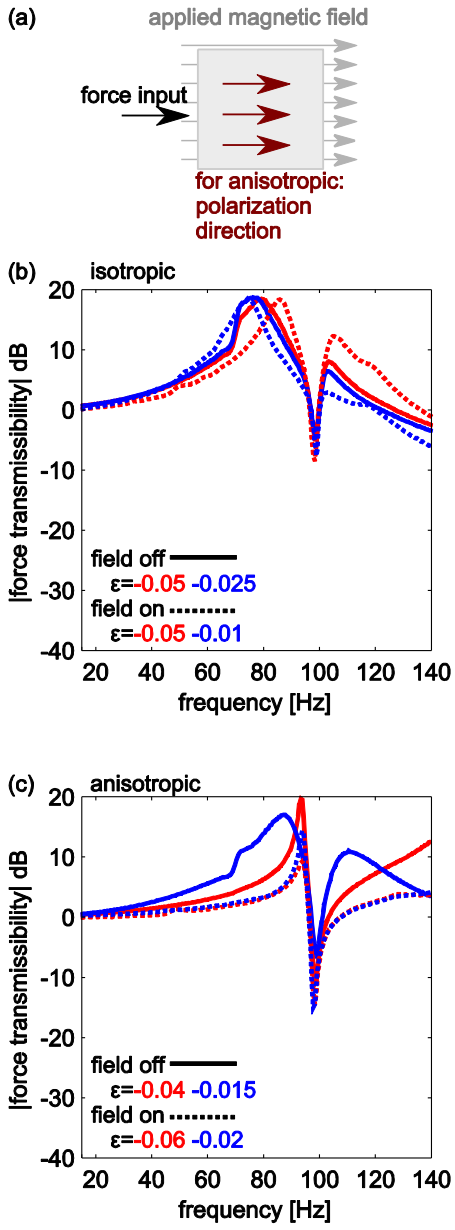

Figure 7. (a) CONTROL SPECIMEN EXAMINATION CONFIGURATION FOR FORCE TRANSMISSIBILITY AND RESULTS FOR (b) ISOTROPIC AND (c) ANISOTROPIC SPECIMENS UNDER TWO DIFFERENT PRE-STRAIN CONDITIONS. VARIOUS PRE-STRAIN APPLICATIONS ARE DENOTED BY THE VALUES ε.

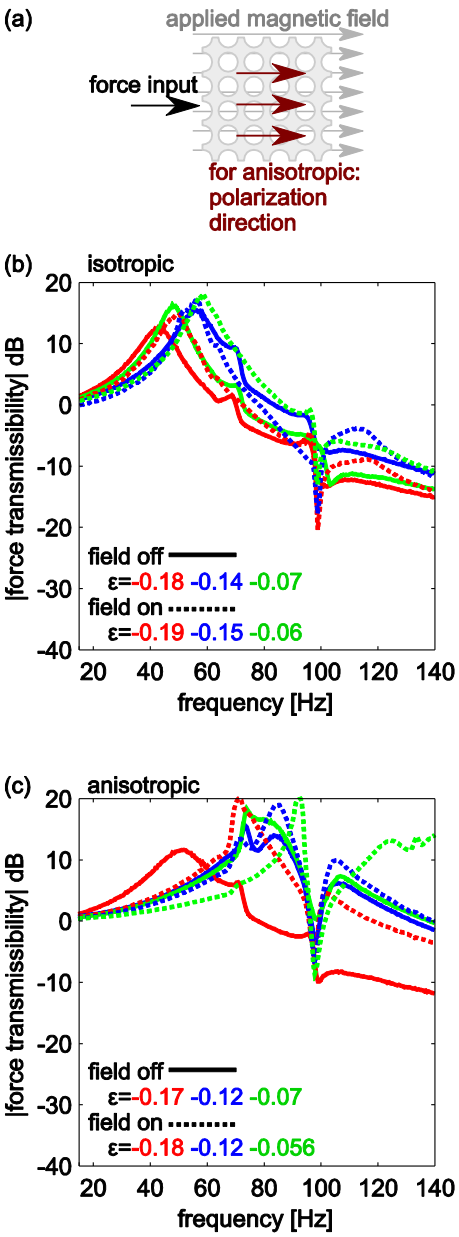

Figure 8. (a) MM SPECIMEN EXAMINATION CONFIGURATION FOR FORCE TRANSMISSIBILITY AND RESULTS FOR (b) ISOTROPIC AND (c) ANISOTROPIC SPECIMENS UNDER TWO DIFFERENT PRE-STRAIN CONDITIONS. VARIOUS PRE-STRAIN APPLICATIONS ARE DENOTED BY THE VALUES ε.

the applied field. In Fig. 7(b), it is evident that the isotropic control specimen uniformly responds to the applied field by stiffening and thus raising the frequency at which the peak force is transmitted. Likewise, it is seen that increased pre-strain results in a nonlinear stiffening effect that produces an increase in the frequency of peak force transmission. The same influences are observed for the anisotropic specimen although the baseline non-strained and without-field cases begin at higher frequencies for the force transmission peak, Fig. 7(c). This is because the specimen is already stiffer due to the anisotropic alignment of the iron particles which is in the direction of the applied force, Fig. 7(a). Thus, the anisotropy also changes the mechanical properties even without the need to tailor the pre-strain or applied magnetic field effects (see Section 3). From Fig. 7(b) and (c), the maximum frequency shift of the peak force transmission is approximately 8%, which occurs due to the introduction of the magnetic field, while in general the amplitudes of the responses are similar throughout the bandwidth of frequencies considered. It is worth noting that the measurements show a sudden drop in force transmission around 100 Hz. Indeed, this trend is observed

in all measurements and is due to the flexibility of the (effectively cantilevered) MDF excitation plunger which results in a narrowband filter effect around 100 Hz that should be neglected in consideration of the dynamic force transmissibility measurements for all specimens due to its uniform occurrence.

Figure 8 shows the resulting magnitudes of force transmissibility for the MM specimens. When the anisotropic specimen is considered, the inherent MM polarization is configured in the same way, respecting the external field, as with the control specimen, Fig. 8(a). For the isotropic specimen without magnetic field, the solid curve measurements in Fig. 8(b) show that without field the increase absolute value of pre-strain ε (i.e. greater compression prior to application of the harmonic driving force) first results in a stiffening and then a softening influence. Namely from ε =-0.07 to -0.14, the peak frequency of force transmission increases from 47 to 55 Hz, while once the pre-strain magnitude increases to -0.18 a significant decrease in this frequency is exhibited, down to 41 Hz while the magnitude is also reduced by about 5 dB. The initial increase of the frequency is associated with the nonlinear stiffening of the specimen for small strains, Fig. 5(d), while the latter decrease is associated with the collapse mechanism, Fig. 1(d). When the magnetic field is applied, the dotted curves in Fig. 8(b) show that the system is initially stiffer but uniformly decreases in stiffness in consequence to increase in pre-strain magnitude. All total, for the isotropic MM specimens, approximately 30 and 20% changes in the peak frequency of force transmission are obtained without and with applied magnetic fields, respectively, due to the utilization of the collapsing mechanism, while the presence of the field tailors the spectral range across which this adaptation may occur. If one leverages the compression and field phenomena concurrently, between the dotted green and solid red curves at 60 Hz, it is evident that almost 20 dB of force transmissibility attenuation can be switched on and off.

For the anisotropic MM specimen, the individual and combined influences of the pre-strain and magnetic field are much more significant. Without the field, the solid curves in Fig. 8(c) show that the increase in pre-strain magnitude from ε =-0.07 to-0.17 results in a uniform drop in the peak frequency of force transmission (approximately 45%) while the amplitude is reduced by 7 dB. Thus, once the collapse has occurred for the anisotropic specimen, at frequencies greater than about 75 Hz a device utilizing the MM would be able to take advantage of the significant attenuation of force at greater excitation frequencies. The general difference in trends between the measurements of the isotropic and anisotropic MM specimens without magnetic field is due to the additional mechanical stiffening effects associated with the aligned iron particles; thus, for the anisotropic MM, the collapse is much more prominent in reducing the local stiffness since it buckles out of the axis in which the alignment occurred. Considering the anisotropic MM specimen in the magnetic field, the dotted curves of Fig. 8(c) show that a 30% swing in the frequency of peak force transmission occurs in consequence to the pre-strain change. Considering the difference between comparable with- and without-field measurements in Fig. 8(c), the anisotropic MM specimen exhibits similar degrees of stiffening by the introduction of the magnetic field for any given pre-strain. Moreover, switching on and off the field can tailor the magnitude of the peak force transmission by approximately 10 dB, as shown in comparing the with- and without-field cases in Fig. 8(c), dotted and solid red curves. By leveraging a combination of intriguing collapse mechanisms due to the metamaterial architecture, and the large susceptibilities to magnetic field by virtue of the anisotropic MRE, the anisotropic MM offers substantially greater properties tuning than that realized by the control specimens.

6 CONCLUSIONS

Using concepts from recent advances in magnetorheological elastomer (MRE) material development and ideas from explorations with cellular, elastic metamaterials, this research has introduced a new concept for magnetoelastic metamaterials (MM) that facilitate large change in mechanical and dynamic properties by topological collapse mechanisms, applied external magnetic fields, or both effects concurrently. Through the experimental studies performed here, the evidence is provided that orders of magnitude adaptation in system performance metrics may be leveraged. For numerous engineering applications where adverse excitation energies upon structural systems vary in amplitude and spectral bandwidth over typical operational scenarios, robust passive-adaptive support devices are sought to alleviate the transmission of wave and vibration energy and thus prevent noise from radiating into the environment. The significant adaptation of properties achieved by the MMs first developed and characterized in this research provide a valuable, non-contact means to provide such performance and functionality.

REFERENCES

1] S.A. Stansfeld and M.P. Matheson, Noise pollution: non-auditory effects on health. British Medical Bulletin 68 (2003) 243-257.

[2] C.Q. Howard, C.H. Hansen, and A. Zander, Vibro-acoustic noise control treatments for payload bays of launch vehicles: discrete to fuzzy solutions. Applied Acoustics 66 (2005) 1235-1261.

[3] P.P. Friedmann, On-blade control of rotor vibration, noise, and performance: just around the corner? Journal of the American Helicopter Society 59 (2014) 041001.

[4] C.E. Hanson, J.C. Ross, and D.A. Towers, "High-speed ground transportation noise and vibration impact assessment," Federal Railroad Administration DOT/FRA/ORD-12/15, (2012).

[5] L. Porter, NASA's new aeronautics research program, in Proceedings of the 45th AIAA Aerospace Sciences Meeting and Exhibit, 2007, pp. 1-49.

[6] E.I. Rivin, Passive Vibration Isolation, ASME Press, New York, 2003.

[7] C. Lewitzke and P. Lee, Application of elastomeric components for noise and vibration isolation in the automotive industry. Transactions Journal of Passenger Cars - Mechanical Systems 110 (2001) 2001-01-1447.
[8] D. Muster and R. Plunkett, "Isolation of vibrations," in Noise and Vibration Control, L.L. Beranek, Ed. Institute of Noise Control Engineering, Washington, D.C., 1988, pp. 406-433.
[9] D. Mayer, J. Militzer, and T. Bein, Integrated solutions for noise and vibration control in vehicles. SAE International Journal of Passenger Cars and Mechanical Systems (2014) 2014-01-2048.
[10] J. Mendoze, K. Chevva, F. Sun, A. Blanc, and S.B. Kim, "Active vibration control for helicopter interior noise reduction using power minimization," National Aeronautics and Space Administration NASA/CR–2014-218147, (2014).
[11] Y. Li, J. Li, W. Li, and H. Du, A state-of-the-art review on magnetorheological elastomer devices. Smart Materials and Structures 23 (2014) 123001.
[12] Y. Li, J. Li, T. Tian, and W. Li, A highly adjustable magnetorheological elastomer base isolator for applications of real-time adaptive control. Smart Materials and Structures 22 (2013) 095020.
[13] C. Chen and W.H. Liao, A self-sensing magnetorheological damper with power generation. Smart Materials and Structures 21 (2012) 025014.
[14] Y.T. Choi and N.M. Wereley, Self-powered magnetorheological dampers. Journal of Vibration and Acoustics 131 (2009) 044501.
[15] T. Mullin, S. Deschanel, K. Bertoldi, and M.C. Boyce, Pattern transformation triggered by deformation. Physical Review Letters 99 (2007) 084301.
[16] J. Shim, S. Shan, A. Košmrlj, S.H. Kang, E.R. Chen, J.C. Weaver, and K. Bertoldi, Harnessing instabilities for design of soft reconfigurable auxetic/chiral materials. Soft Matter 9 (2013) 8198-8202.
[17] C.R. Tipton, E. Han, and T. Mullin, Magneto-elastic buckling of a soft cellular solid. Soft Matter 8 (2012) 6880-6883.
[18] A. Bayat and F. Gordaninejad, Band-gap of a soft magnetorheological phononic crystal. Journal of Vibration and Acoustics 137 (2015) 011011.
[19] A. Bayat and F. Gordaninejad, Dynamic response of a tunable phononic crystal under applied mechanical and magnetic loadings. Smart Materials and Structures 24 (2015) 065027.